Published in final edited form as:
J Med Chem. 2012 March 8; 55(5): 2406–2415. doi:10.1021/jm201690h.

Radiosynthesis and evaluation of an ^{18}F-labeled positron emission tomography (PET) radioligand for brain histamine subtype-3 receptors based on a nonimidazole 2-aminoethylbenzofuran chemotype

Xiaofeng Bao, **Shuiyu Lu**, **Jeih-San Liow**, **Sami S. Zoghbi**, **Kimberly J. Jenko**, **David T. Clark**, **Robert L. Gladding**, **Robert B. Innis**, and **Victor W. Pike***
Molecular Imaging Branch, National Institute of Mental Health, National Institutes of Health, Building 10, Rm. B3 C346A, 10 Center Drive, Bethesda, Maryland, 20892, United States

Abstract

A known chemotype of H_3 receptor ligand was explored for development of a radioligand for imaging brain histamine subtype 3 (H_3) receptors in vivo with positron emission tomography (PET), namely non-imidazole 2-aminoethylbenzofurans, represented by the compound (*R*)-(2-(2-(2-methylpyrrolidin-1-yl)ethyl)benzofuran-5-yl)(4-fluorophenyl)methanone (**9**). Compound **9** was labeled with fluorine-18 ($t_{1/2}$= 109.7 min) in high specific activity by treating the prepared nitro analog (**12**) with cyclotron-produced [^{18}F]fluoride ion. [^{18}F]**9** was studied with PET in mouse and in monkey after intravenous injection. [^{18}F]**9** showed favorable properties as a candidate PET radioligand, including moderately high brain uptake with a high proportion of H_3 receptor-specific signal in the absence of radiodefluorination. The nitro compound **12** was found to have even higher H_3 receptor affinity, indicating the potential of this chemotype for the development of further promising PET radioligands.

Keywords

Radioligand; H_3 receptor; PET; imaging; fluorine-18

INTRODUCTION

The histamine subtype 3 (H_3) receptor is one of the four G-protein-coupled receptors of the histamine receptor family.[1–3] H_3 receptors are widely expressed in the mammalian brain and regulate the pre-synaptic release of histamine and other neurotransmitters, such as acetylcholine, noradrenalin and dopamine. Brain H_3 receptors are attractive drug targets for the treatment of cognitive and other disorders, such as narcolepsy, attention-deficit hyperactivity disorder, and pain.[4,5]

The use of selective H_3 receptor radioligands with PET (positron emission tomography) has potential *i*) to elucidate any changes in the distribution and density of H_3 receptors in living human brain during the progression of neuropsychiatric disorders, and *ii*) to determine the dose-dependence of extent and duration of brain H_3 receptor occupancy by candidate drugs that may be directed at the treatment of such disorders.[6] So far, few radioligands have been

*Corresponding author, Phone (301) 594 5986, FAX (301) 480 5112, pikev@mail.nih.gov.

Supporting Information Available: Chromatograms for the separation and analysis of [^{18}F]**9**. This material is available free of charge via the Internet at http://pubs.acs.org.

prepared and evaluated for imaging brain H_3 receptors with PET. These radioligands may be structurally categorized as imidazoles, such as [^{18}F]FUB 272 ([^{18}F]**1**)[7], [^{18}F]VUF 5000 ([^{18}F]**2**)[8,9] , [^{18}F]fluoroproxyfan ([^{18}F]**3**)[10,11], [^{11}C]UCL 1829 ([^{11}C]**4**)[7] or non-imidazoles, such as [^{11}C]JNJ-10181457 ([^{11}C]**5**)[12], [^{11}C]GSK189254 ([^{11}C]**6**)[13,14], [^{11}C]Merck 1b ([^{11}C]**7**)[15] and [^{18}F]Merck 2b ([^{18}F]**8**)[15] (Chart 1). The imidazoles have not shown encouraging results. Only the non-imidazoles [^{11}C]**6**, [^{11}C]**7** and [^{18}F]**8** have shown promise in animal experiments and only [^{11}C]**6** is known to have progressed to studies in human subjects[14].

In our efforts to develop an ^{18}F-labeled H_3 receptor PET ligand, we selected a new chemotype, the reported non-imidazole 2-aminoethylbenzofuran-based H_3 receptor antagonist/inverse agonist **9**,[16] for radiolabeling and evaluation in animals. Ligand **9** appeared attractive as a candidate for development as a PET radioligand because it was already known to exhibit some of the properties recognized as being desirable,[17–20] including high affinity and selectivity for binding to target human receptors, ability to cross the blood-brain-barrier, and potential to be labeled with no-carrier-added (NCA) fluorine-18 ($t_{1/2}$ = 109.7 min) at an aryl carbon.[21] Here we report the radiosynthesis of [^{18}F]**9** and an evaluation of its radioligand behavior in mouse and monkey. Our findings show [^{18}F]**9** is an effective H_3 receptor radioligand.

RESULTS AND DISCUSSION

Chemistry

Reference ligand **9** was prepared from commercially available (4-fluorophenyl)(4-hydroxyphenyl)methanone, as described previously.[16] We prepared the nitro analogue **12** to provide a precursor suitable for use in a single-step labeling of **9** with cyclotron-produced NCA [^{18}F]fluoride ion because *p*-nitrophenylketones are well known to be susceptible to aromatic nucleophilic substitution with [^{18}F]fluoride ion.[21,22] The synthesis of **12** was analogous to that known[16] for the fluoro compound **9** (Scheme 1). An initial attempt to demethylate the commercially available (4-methoxyphenyl)(4-nitrophenyl)methanone with NaSMe in DMF[23,24] proved unsuccessful due to substitution of the nitro group to form a thioether. This observation nevertheless confirmed the susceptibility of the nitro group towards aromatic nucleophilic substitution. Selective demethylation of (4-methoxyphenyl)(4-nitrophenyl)methanone to the required (4-hydroxyphenyl)(4-nitrophenyl)methanone (**10**) was readily achieved by use of a non-nucleophilic Brøsted acid reagent, HBr in AcOH.[25,26] Treatment of **10** with 0.5 equivalents of iodine and potassium iodide selectively produced **11** having iodine in ortho position to the hydroxy group in a moderate yield (30%) Use of a sub-stoichiometric amount of iodine reduced the unwanted di-iodination that we observed from the use of a stoichiometric amount of iodine. 1-(3-Butynyl)-2(*R*)- methylpyrrolidine[16] was used directly as a MeCN solution (~ 0.1 M) for ring closure with **11** to give the target nitro precursor **12** in useful yield (28%).

Pharmacological assays and screen

Assay of compound **9** for binding to human recombinant H_3 receptors, expressed in HEK293T cells, confirmed high affinity with K_i in the nanomolar range (Table 1). The affinities of **9** for a wide range of other human recombinant receptors and binding sites, including the other sub-types of histamine receptor, were found to be at least 200-fold lower. These results accord with the previous report of the selectivity of **9** for binding to H_3 receptors among a wide battery of receptors ($H_{1\text{-}4}$, $D_{1,2s,2,4,}$ $5\text{-}HT_{1—3}$, adrenergic and muscarinic) and transporters (NET, DAT, SERT) binding sites from unidentified species.[16] Therefore, **9** exhibited the necessary high human H_3 receptor affinity and selectivity for consideration as a candidate PET radioligand. The nitro precursor **12** was similarly screened

and was found to have almost five-fold higher affinity for human H_3 receptors, and also greater than 200-fold selectivity for all other tested receptors and binding sites (Table 1).

Intrinsic activity may influence the utility of a PET radioligand for imaging G-protein coupled neuroreceptors. For example, antagonists are expected to bind to the full population of target receptors whether present in the G-protein coupled state or not, whereas agonists might be expected to bind only to the sub-population of receptors in the G-protein coupled state. Ligand **9** was reported to be a competitive H_3 receptor antagonist in a variety of assays, including a Ca^{2+} flux assay, and also found to be a potent H_3 receptor inverse agonist for GTP-γ-S binding in H_3 receptor-transfected cells.[16] Both **9** and **12** were found to be inverse agonists in a GTP-γ-S assay performed by the Psychoactive Drug Screening Program.

Radiochemistry

[^{18}F]**9** was produced automatically within a lead-shielded hot-cell from cyclotron-produced [^{18}F]fluoride ion (200—300 mCi) in a Synthia device[27] equipped with a microwave heater (Scheme 2).[28] In trial experiments, reaction of **12** with [^{18}F]fluoride ion in DMF gave a higher decay-corrected radiochemical yield (RCY) of [^{18}F]**9** (34%) than in MeCN (2%) or in DMSO (6%). In these experiments, microwave power was set between 50 and 60 W so that reaction temperature did not exceed 90 °C because decomposition of [^{18}F]**9** became significant above 100 °C. [^{18}F]**9** was separated with single-pass reverse phase HPLC in high radiochemical purity (> 99%). The pharmacologically active precursor **12** eluted at 29.1 min, and was well separated from [^{18}F]**9** (t_R = 36.0 min). No residual **12** or other chemical impurity was detected in the formulated radioligand by analytical HPLC. The specific radioactivity of [^{18}F]**9**, when finally formulated for intravenous injection at about 110 min from the end of radionuclide production, was 1311 ± 221 mCi/μmol (n = 12). The average RCY of formulated [^{18}F]**9** was 9.3 ± 5.8% (n = 12).

Measurement of $LogD_{7.4}$ and Computation of cLogD and cLogP

The lipophilicity of a candidate radioligand is an important consideration[17–20,29,30] since this property strongly influences i) ability of a radioligand to penetrate the blood-brain barrier, ii) non-specific binding of the radioligand in brain, iii) the magnitude and measurability of the plasma free fraction (f_P), a parameter which may need to be known for the application of certain types of PET data quantitative analyses, and iv) general susceptibility of a radioligand to metabolism. Moderate lipophilicity is usually considered desirable for achieving adequate blood-brain barrier penetration without incurring unacceptable non-specific binding, and for avoiding troublesome lipophilic brain-penetrant radiometabolites[29] and low f_P.[30] The measured $LogD_{7.4}$ of [^{18}F]**9** was 2.95 ± 0.06 (n = 6). Thus, the lipophilicity of **9** was found to be within the desirable range of LogD 1.5–3.5.[19] Computed cLogD (at pH = 7.4) values of **9** and **12** were 2.90 and 2.45, respectively, and hence Pallas software appears quite accurate for predicting lipophilicity for this type of structure. Computed LogP values for **9** and **12** were 4.79 ± 0.43 and 4.34 ± 0.34.

PET imaging of [^{18}F]9 in mice

Mouse brain is known to contain relatively i) high densities of H_3 receptors in striatum, parietal cortex, insular cortex, nucleus acumbens, globus pallidus, and olfactory tubercle, ii) moderate densities in thalamus, hypothalamus, and hippocampus, and iii) low densities in cerebellum and brain stem.[31,32] H_3 receptor concentrations in striatum have been reported to be 95 fmol/mg tissue, which approximates to 95 nM.[31] A practical guideline[19] is that for successful imaging with PET radioligands that are intended to bind reversibly to target receptors, B_{max}/K_d should exceed 10 *in vivo*. [^{18}F]**9** has a K_i value of 1.0 nM for rodent (rat)

H_3 receptors[16] and therefore, the density of H_3 receptors (B_{max}, 95 nM) should be adequate for PET imaging with this radioligand.

Brain time-activity curves of [^{18}F]**9** in mice were acquired at baseline, and after pretreatment of mice with the selective high-affinity H_3 inverse agonist ciproxifan[33] (2.0 mg/kg, i.v.), nitro precursor **12** (2.0 mg/kg, i.v.), or ligand **9** itself (1.0 mg/kg, i.v.) (Figure 1). At baseline, radioactivity entered brain quickly after i.v. injection of [^{18}F]**9**, with peak whole brain uptake reaching a quite high level of 3.36 SUV at about 6.5 min. Brain radioactivity concentration then slowly declined to about 2.3 SUV by 90 min. In mice pre-treated with ciproxifan, brain radioactivity concentration quickly peaked at a lower level of about 1.98 SUV at 4.5 min after radioligand injection, and then gradually reduced to 1.09 SUV at 90 min, a value much lower than seen at the same time after radioligand injection in the baseline experiment. When mice were pretreated with either the nitro precursor **12** or the ligand **9** itself, brain radioactivity peaked at 3.5 min and at higher values of 4.34 or 4.07 SUV respectively. Brain radioactivity then decreased quickly to < 1.20 SUV at 90 min, a level similar to that in the ciproxifan pre-block experiment. Together, these data indicate that at baseline a high proportion of radioactivity in whole brain represents specific binding of [^{18}F]**9** to H_3-receptors.

The reasons for the differences in brain radioactivity uptake between the pre-treatment experiments with ciproxifan and those using the structural congeners **12** and **9** are unclear. All three ligands appear to be highly selective for H_3 receptors. One possibility is that at their administered doses **12** and **9** displace the structurally similar [^{18}F]**9** from plasma proteins, giving a higher plasma free fraction (f_P) and greater entry of radioligand into brain than in the baseline experiment. Another possibility is that **12** or **9**, but not ciproxifan, displaces [^{18}F]**9** from other unknown binding sites in periphery, thereby increasing availability of radioligand for brain entry. However, the cumulative in vitro data on the strong selectivity of both **12** and **9** for binding to H_3 receptors argue against this possibility. H_3 receptors also exist in peripheral organs such as lung and gastrointestinal tract.[1] The administered doses of the agents **9** and **12** may be more effective than that of ciproxifan at blocking the binding of [^{18}F]**9** to peripheral H_3 receptors, thereby increasing the free concentration of [^{18}F]**9** in plasma and hence uptake of radioactivity into brain. The imaging results, showing that [^{18}F]**9** gives a strong H_3-receptor specific signal in mice, encouraged our further evaluation of [^{18}F]**9** in non-human primate.

PET imaging of [^{18}F]9 in monkey

The distribution of H_3 receptors in rhesus monkey brain is similar to that in human brain.[15,34] As in rat, H_3 receptors are enriched in basal ganglia, and also present in hippocampus and cortical areas, whereas cerebellum has lower levels of H_3 receptors.

Brain time-activity curves of [^{18}F]**9** in male rhesus monkey were acquired at baseline (Figure 2A), and after treatment with ciproxifan (2.0 mg/kg, i.v.) or **9** (1.0 mg/kg, i.v.) (Figure 2B). After injection of [^{18}F]**9** at baseline, radioactivity entered brain well with peak uptake in H_3 receptor-rich regions, such as striatum (4.45 SUV) and frontal cortex (3.86 SUV), occurring at about 27.5 and 47.5 min, respectively. Peak radioactivity concentration in other regions was lower but still higher than in cerebellum (2.76 SUV). The concentration of radioactivity in all regions slowly and continuously decreased to the end of the PET experiment (180 min).

Summed PET images of monkey brain at baseline showed a distribution of radioactivity reflecting the expected distribution of H_3 receptors (Figure 3), with no evidence of radioactivity uptake into skull.

Pre-treatment of monkeys with ciproxifan reduced the peak radioactivity concentration in H_3 receptor-rich regions such as frontal cortex and striatum, but not in cerebellum. Subsequent washout of radioactivity from all H_3 receptor containing regions was slow. Pre-treatment with **9** reduced peak radioactivity concentrations in all brain regions and thereafter all brain region concentrations declined to a common low level at 180 min. The summed PET images from pretreatment experiments with **9** show a uniform low distribution of radioactivity across brain, again with no evidence of radioactivity uptake in skull. Thus, pretreatment with **9** appeared more effective than pretreatment with ciproxifan in showing specific binding of [^{18}F]**9** in monkey brain.

Ciproxifan is known to show species differences in H_3 binding affinity, with over 100-fold lower affinity for human H_3 receptors (K_i = 63 nM) than for rat H_3 receptors (K_i = 0.51 nM). The binding affinity of ciproxifan for monkey H_3 receptors is unknown. There is a possibility that the affinity of ciproxifan for monkey H_3 receptors is similar to that for human H_3 receptors and this may account for incomplete blockade of the brain H_3 receptors at the administered dose.

Stability of [^{18}F]9 in buffer, whole blood and plasma in vitro

[^{18}F]**9** was found to be 98.8 ± 0.2% (n = 6) unchanged after 2.5 h in sodium phosphate buffer (pH 7.4) at room temperature, and was also stable in monkey whole blood (98.4% ± 0.07%, n = 6) and monkey plasma (99.2% ± 0.1%, n = 6) at room temperature in vitro for 2.5 h. Therefore, accurate measurement of unchanged radioligand and radiometabolites in plasma was feasible by radio-HPLC, for the ultimate purpose of generating radioligand arterial input functions.

Emergence of radiometabolites of [^{18}F]9 in monkey plasma in vivo

In the analyses of all studied monkey plasma samples, extractions of radioactivity from plasma with acetonitrile for radio- HPLC analysis were very effective (95.3 ± 7.44%, n = 115). After administration of [^{18}F]**9** into monkey at baseline, radioactivity cleared rapidly from plasma until about 50 min when the low level of decay-corrected plasma radioactivity concentration became almost constant (Figure 4). Similar plasma time-radioactivity curves were seen in monkey that had been pre-treated with ciproxifan or **9** (Figure 4). HPLC analyses of plasma showed that the concentration of unchanged radioligand declined continuously (Figure 4) while three radiometabolites [^{18}F]**A**—**C** emerged (Figure 5). These radiometabolites appeared to be less lipophilic than [^{18}F]**9** (t_R = 5.63 min) according to their shorter retention times on reverse phase HPLC (Figure 6). Radiometabolites emerged similarly in plasma of monkeys pretreated with ciproxifan (Figure 5). By contrast, in monkeys pretreated with **9,** parent radioligand more quickly decreased to become the minor component in plasma. In these experiments, the least lipophilic radiometabolite [^{18}F]**A** became the major component in plasma. The ability of the radiometabolites to penetrate the blood-brain barrier is presently unknown. Nonetheless, because of their lower lipophilicities, these radiometabolites might be expected to enter brain less readily than parent radioligand. They would not therefore be expected to be troublesome to quantification of radioligand binding to H_3 receptors.

The routes of radioligand metabolism and the identities of the radiometabolites are also unknown. However, a close analog of **9** having a nitrile (CN) group in place of the fluoro (F) group has been found to be a substrate for CYPs 3A4, 1A2 and 2D6, as well as flavin monooxygenases FMO-1 and FMO-3.[16] The lack of radioactivity uptake in skull (Figure 3) indicates that none of the radiometabolites of [^{18}F]**9** is [^{18}F]fluoride ion, and that radiodefluorination does not occur for this radioligand. Radioligands that radiodefluorinate

may give high radioactivity uptake in skull which may compromise PET measurements in nearby brain through 'partial volume effects'.

Plasma Free Fraction of [^{18}F]9

The plasma free fraction (f_P) of [^{18}F]**9** in monkey plasma was accurately measurable and found to be 2.08 ± 0.14% at baseline and 1.4 ± 0.1% during pre-treatment with **9**.

Biomathematical analysis of PET data acquired with [^{18}F]9

Time-activity curves in baseline monkey experiments with [^{18}F]**9** fitted quite well to both one-tissue (1TC) and two tissue (2TC) compartmental models. An F test showed that the 2TC model gave the best fit to acquired data (Figure 7). Application of 2TC modeling of the data from the two monkeys showed that on average ciproxifan reduced the V_T ranging 26—34% whilst **9** reduced V_T around 49—58% (Table 2). These data indicate that the majority of radioactivity in H_3 receptor-rich regions of brain represents specific binding of [^{18}F]**9** to H_3 receptors.

By truncating acquired PET data we obtained V_T values for different time periods after radioligand injection. Reasonably stable V_T values were obtained from data acquired between 130 and 180 min (Figure 8), suggesting that for this radioligand in monkey, the ingress of troublesome radiometabolites into brain is not greatly problematic.

Comparison of [^{18}F]9 with other H_3 receptor radioligands

The only other ^{18}F-labeled radioligand for brain H_3 receptors that has been reported to give a sizable receptor-specific signal in vivo is [^{18}F]**8** (Chart 1).[15] In rhesus monkey, this radioligand gives much lower peak brain radioactivity uptake (< 1.3 SUV) in H_3 receptor–rich regions than [^{18}F]**9** (~ 4.5 SUV; Figure 2), although a somewhat higher proportion (~75%) of this lower radioactivity uptake appears to be receptor-specific binding. [^{18}F]**8** is labeled in a fluoromethoxy position which may be susceptible to radiodefluorination in human subjects in vivo to give high radioactivity uptake in bone including skull. Skull uptake of radioactivity is known to occur for other PET radioligands labeled with fluorine-18 in a fluoromethoxy position, including (*S*,*S*)-[^{18}F]FMeNER-D$_2$ [35] and [^{18}F]FMEPEP-d_2 [36]. In fact the incorporation of deuterium into these radioligands is intended to counter radiodefluorination *in vivo*. We found that [^{18}F]**9** shows no radiodefluorination in monkey. [^{18}F]**9** would not be expected to be radiodefluorinated in human subjects because aryl carbon-^{18}F bonds are usually stable in vivo. The radioligand [^{11}C]**7**, has higher peak brain uptake (~2.3 SUV) than [^{18}F]**8**, but this is still lower than that of [^{18}F]**9**. However, [^{11}C]**7** appears superior in giving a very high proportion (~ 83%) of H_3 receptor-specific binding. The radioligand [^{11}C]**6** gave very high peak uptake in pig brain and a very high proportion (>90%) of H_3 receptor-specific signal.[13] So far this is the only H_3 receptor radioligand studied in human subjects.[14] In baseline human experiments this radioligand demonstrates progressively increasing radioactivity uptake in H_3 receptor-rich regions, apparently due to a slow off rate from the receptor. Although this high-affinity radioligand can be used to measure drug receptor occupancy, care has to be taken to avoid mass effects of co-administered carrier in the use of this radioligand, and in particular undesirably significant and prolonged occupancy of H_3 receptors by carrier.

CONCLUSIONS

[^{18}F]**9** demonstrates favorable properties as a PET radioligand for brain H_3 receptors in monkey, including moderately high brain uptake and sizeable receptor-specific signal in the absence of radiodefluorination. Moreover, this study shows that higher affinity ligands, such

as **12,** exist among this chemotype,[16] which may thus serve as a platform for developing further improved ^{11}C-labeled and ^{18}F-labeled H_3 receptor PET radioligands.

EXPERIMENTAL SECTION

Animal Procedures

All animal experiments were performed in accordance with the *Guide for Care and Use of Laboratory Animals*[37] and were approved by the National Institute of Mental Health Animal Care and Use Committee.

Materials and General Methods

All reagents and solvents were ACS grade or higher and used without further purification. Unless otherwise noted, all chemicals were purchased from Sigma- Aldrich (Milwaukee, WI). Reactions were performed under argon atmosphere with standard Schlenk techniques. 1-(3-Butynyl)-2-(*R*)-methylpyrrolidine was synthesized with a published method[16] from (*R*)-2-methylpyrrolidine and 3-butynyl-4-toluenesulfonate; this reagent was used as a ~ 0.1 M solution in MeCN without purification. Ligand **9** was prepared from commercially available (4- flourophenyl)(4-hydroxyphenyl)methanone, as described previously,[16] and obtained as a brown oil in >99 % chemical purity.

^{1}H (400 MHz), ^{13}C NMR (100 MHz) and ^{19}F NMR (376 MHz) spectra were recorded on an Avance 400 spectrometer (Bruker; Billerica, MA). Chemical shifts are reported in δ units (ppm) downfield relative to the chemical shift for tetramethylsilane. Abbreviations br, s, d, t and m denote broad, singlet, doublet, triplet, and multiplet, respectively. GC-MS spectra were obtained on a Polaris-Q GC-MS instrument (Thermo Fisher Scientific Corp., Waltham, MA). LC-MS was performed on a LCQ Deca instrument (Thermo Fisher Scientific Corp.) equipped with a reverse-phase HPLC column (Luna C18, 3 [m, 50 mm × 2 mm; Phenomenex, Torrance, CA), eluted at 200 [L/min with a mixture of A (H_2O-MeOH-AcOH, 90: 10: 0.5 v/v) and B (MeOH-AcOH, 100: 0.5 v/v), initially composed of 20% B and linearly reaching 80% B in 3 min). High resolution mass spectra (HRMS) were acquired at the Mass Spectrometry Laboratory, University of Illinois at Urbana-Champaign (Urbana, IL) under electron ionization conditions with a double-focusing high resolution instrument (Autospec; Micromass Inc.). Thin layer chromatography was performed on silica gel layers (type 60 F254; EMD Chemicals, Gibbstown, NJ), and compounds were visualized under UV light (λ =254 nm). Prepared compounds were analyzed by HPLC on a Prodigy column (10μm, 4.6 mm × 250 mm; Phenomenex) eluted with 85%B at 2 mL/min with eluate monitored for absorbance at 243 nm (Gold 168 detector; Beckman) and were of > 95% purity.

(4-Hydroxyphenyl)(4-nitrophenyl)methanone (10)

(4-Methoxyphenyl)(4- nitrophenyl)methanone (150 mg, 0.58 mmol) was suspended in hydrobromic acid (5 mL, 48% w/w)[25,26] and glacial acetic acid (5 mL). The mixture was refluxed for 9 h, and then taken to dryness under vacuum. The residue was dissolved in EtOAc and extracted with H_2O. The organic layer was dried with $MgSO_4$. After removal of solvent, flash chromatography (silica gel; EtOAc/hexane, 20:80, v/v) of the residue gave **10** as a gray solid (122 mg, 87%). M.p. 198–200 °C. ^{1}H NMR (CD_3OD): *δ*8.24 (d, 2H, J = 8.8 Hz), 7.77 (d, 2H, *J* = 8.8 Hz), 7.62 (d, 2H, *J* = 8.8 Hz), 6.79 (d, 2H, *J* = 8.8 Hz). ^{13}C NMR (CD_3OD): *δ*195.39, 164.44, 150.94, 145.42, 134.14, 131.38, 128.96, 124.50, 116.49 ppm. GC-MS: found 243.00 (M^+); calcd for $C_{13}H_9NO_4$, 243.05.

(4-Hydroxy-3-iodophenyl)(4-nitrophenyl)methanone (11)

A solution of **10** (500 mg, 2.05 mmol) in NH_4OH (1 M, 17.1 mL) was stirred at 25 °C for 15 min and then treated with an aqueous solution (2.05 mL) of KI (1.69 g, 10.25 mmol) and I_2 (259 mg, 1.03 mmol) with stirring at 25 °C for 48 h. Solids were filtered off, dissolved in ethyl acetate, and then washed with H_2O and brine. The organic layer was dried with $MgSO_4$. After removal of solvent, flash chromatography (silica gel; EtOAc/hexane, 50:50 v/v) of the residue gave **11** as pale yellow solid (190 mg, 26%). M.p. 248–250 °C. ^{1}H NMR (DMSO-d_6/CD_3OD): δ8.31 (d, 2H, J = 8.4 Hz), 8.09 (s, 1H), 7.84 (d, 2H, J = 7.6 Hz), 7.62 (d, 1H, J = 8.4 Hz), 6.94 (d, 1H, J = 8.4 Hz). ^{13}C NMR (DMSO-d_6): δ192.37, 162.25, 149.74, 143.75, 141.81, 133.00, 130.89, 129.48, 124.19, 115.03, 85.61 ppm. GC-MS: found 368.77 (M^+); calcd for $C_{13}H_8INO_4$, 368.95.

(*R*)-(2-(2-(2-Methylpyrrolidin-1-yl)ethyl)benzofuran-5-yl)(4-nitrophenyl)methanone)12)

Compound **11** (0.500 g, 1.36 mmol) and a solution of 1-(3-butynyl)-2-(*R*)-methylpyrrolidine (0.1M) in MeCN (16.9 mL) were mixed in a round-bottomed flask (100-mL). $Pd(OAc)_2$ (9.0 mg, 0.04 mmol), tri-*p*-tolylphosphine (24.3 mg, 0.08 mmol), and CuI (77 mg, 0.40 mmol) were added. The resultant mixture was stirred at 25 °C for 10 min. *i*-Pr_2NH (1.9 mL, 13.6 mmol) was then added and the mixture heated at 60 °C for 16 h. The reaction mixture was allowed to cool and filtered through a plug of Celite. The filtrate was concentrated under reduced pressure. Flash chromatography (silica gel; CH_2Cl_2/MeOH/NH_4OH, 90: 9.9: 0.1 by vol.) of the residue gave **12** as a dark brown semi-solid (143 mg, 28%). ^{1}H NMR ($CDCl_3$): δ8.35 (d, 2H, J = 6.8 Hz), 7.94 (m, 3H), 7.75 (d, 1H, J = 8.4 Hz), 7.53 (d, 1H, J = 8.4 Hz), 6.56 (s, 1H), 3.27 (m, 2H), 3.06 (t, 2H, J = 8.4 Hz), 2.54 (m, 1H), 2.44 (m, 1H), 2.26 (m, 1H), 1.98 (m, 1H), 1.80 (m, 2H), 1.48 (m, 1H), 1.16 (d, 3H, J = 6.0 Hz) ppm. ^{13}C NMR ($CDCl_3$): δ194.61, 159.80, 157.43, 149.54, 143.77, 131.25, 130.55, 129.09, 125.97, 123.68, 123.44, 111.08, 103.14, 60.34, 53.76, 51.60, 32.58, 27.90, 21.66, 18.70 ppm. LCMS (M^++1) 379.1; HRMS (M^++1) found, 379.1668; calcd for $C_{22}H_{23}N_2O_4$, 379.1658. HPLC: t_R = 12.7 min, purity > 99%.

Production of NCA [^{18}F]fluoride ion reagent

NCA [^{18}F]fluoride ion was produced by irradiating ^{18}O-enriched water (98 atom %) with a beam (20 [A) of 16.5 MeV protons[38] from a PETrace cyclotron (GE, Uppsala, Sweden) for 120 min. At the end of irradiation, the aqueous solution (20—200 μL) of [^{18}F]fluoride ion (20—200 mCi) was transferred in a glass V-vial (1-mL) to a lead-shielded hot-cell and placed in the cavity of a model 521 instrument for accelerated microwave chemistry (Resonance Instruments Inc., Skokie, IL). The latter is integrated with a Synthia MKII radiochemistry platform inside the same hot-cell, as described previously.[28] A solution of K_2CO_3/K 2.2.2 (100 μL stock solution of 0.5 mg K_2CO_3 and 5.0 mg K 2.2.2 in 9:1 MeCN and H_2O mixture) and MeCN (600 μL) were added to the V-vial, which was then placed under N_2 gas flow (200 mL/min) and irradiated with microwaves (90 W in 2 × 2 min pulses). The addition of acetonitrile (600 [L) followed by microwave irradiation was repeated three times to give dry NCA [^{18}F]fluoride ion-K^+- K 2.2.2 reagent.

Radiosynthesis of [^{18}F]9

Precursor **12** (1.0 mg) in DMF (0.3 mL) was introduced into the vial containing anhydrous [^{18}F]fluoride ion-K^+-K 2.2.2 and irradiated with microwaves (50—55 W) in 3 × 2 min pulses. The reaction temperature was carefully held between 80 and 90 °C during the irradiation. The reaction mixture was then diluted with water (0.7 mL) and injected onto a reverse phase column (Prodigy, 10 [m, 10 mm × 250 mm; Phenomenex) eluted at 6 mL/min with a mixture of aq. NH_4OH (0.025%, pH 8.5) (A, 70%) and MeCN (B, 30%). B was kept at 30% for 5 min, linearly increased to 70% over 3 min, and then held at 70% for 45 min.

The collected fraction of [^{18}F]**9** (t_R, 34—36 min) was transferred to a pear-shaped flask and the solvent removed under vacuum. The residue was diluted with sterile saline for injection (10 mL) containing EtOH (10%; USP grade), and passed through a sterile filter (2.5 μm, Millex MP, Millipore, Bedford, MA). The pH of the final dose was in the range 6—8.

RCY was calculated from the radioactivity of formulated [^{18}F]**9**. Chemical and radiochemical purities, and specific radioactivity were determined by reverse phase HPLC on a Prodigy column (10 [m, 4.6 mm × 250 mm; Phenomenex) eluted with 20% A and 80%B at 2 mL/min with eluate monitored for absorbance at 243 nm (Gold 166 detector, Beckman) and for radioactivity (PMT, HC- 003; Bioscan Inc, Washington DC). [^{18}F]**9** (t_R = 17.9 min) was identified by, i) coelution with nonradioactive reference **9** in the aforementioned analytical HPLC method, and ii) LC-MS analysis of associated carrier for comparison with that of reference **9** (*m/z* = 352 (M^++1)).

Computation of cLogP and cLogD, and Measurement of LogD

cLogP and cLogD (at pH = 7.4) values for **6** were computed with the program Pallas 3.0 for Windows (CompuDrug; S. San Francisco, CA). The LogD value of [^{18}F]**9** was measured as the log of its distribution coefficient between *n*-octanol and sodium phosphate buffer (0.15 M, pH 7.4), as described previously.[39,40] [^{18}F]**9** was shown to be stable to buffer by radio-HPLC analysis. The radioactivity in the organic phase and that in the aqueous phase were counted in a γ-counter. Counting errors were < 0.3 ± 0.1% (*n* = 6) at one standard deviation.

PET imaging of [^{18}F]9 in mouse

Wild type FVB mice (Taconic Farm, Germantown, NY) were anesthetized with 1.5% isoflurane in oxygen, and body temperatures were maintained at 36.5—37.0 °C with a heating lamp. Intravenous injections were performed via polyethylene cannulae (PE-10; Becton Dickinson, Franklin Lakes, NJ) in the tail vein. The cannulae were secured with tissue adhesive (Vetbond; 3M, St. Paul, MN). Thirteen mice (27.6 ± 3.8 g) were scanned either at baseline (*n* = 4) or after treatment with ciproxifan (2.0 mg/kg, i.v.; *n* = 3), **9** (1.0 mg/kg, i.v.; *n* = 3) or **12** (1.0 mg/kg, i.v.; *n* = 3) 30 min before injection of [^{18}F]**9**.

Serial dynamic scans were acquired with a Focus 120 microPET scanner (Siemens Medical Solutions, Knoxville, TN) started at the time of injection of NCA [^{18}F]**9** (73 ± 29 [Ci) and were continued for 120 min with increasing frame durations from 20 s to 20 min. Images were reconstructed by a Fourier rebinning/2D ordered-subset expectation maximization algorithm. No attenuation or scatter correction was applied. Whole brain decay-corrected time-activity curves were generated using PMOD 3.0 (PMOD Technologies, Zurich, Switzerland). Brain uptake of radioactivity was expressed as standardized uptake value (SUV) where SUV = (% injected dose per cm^3 brain) × (g body weight).

PET imaging of [^{18}F]9 in monkey

Four male rhesus monkeys (7.3 ± 0.8 kg) were used for PET scans of the brain. Two of the monkeys had femoral artery indwelling catheters for blood sampling. All four monkeys were studied at baseline (*n* = 4), three at 30 min after treatment with ciproxifan (2.0 mg/kg, i.v.) and two at 30 min after treatment with **9** (1.0 mg/kg, i.v.). All monkeys were immobilized with ketamine (10 mg/kg, i.m.) and maintained in anesthesia with 1.5% isoflurane in O_2 via an endotracheal tube. NCA [^{18}F]**9** (3.91 ± 0.46 mCi, *n* = 9) was injected intravenously. All PET scans were acquired with a Focus 220 microPET scanner (Siemens Medical Solutions, Knoxville, TN) for 180 min except one scan for 120 min. Each scan consisted of 45 frames of increasing duration, from 30 s to 5 min. Images were reconstructed with a Fourier rebinning/2D filtered back projection algorithm with scatter and attenuation correction. All data were decaycorrected to the time of radioligand injection.

With a view to analyzing monkey plasma for radiometabolites and thereby measuring an arterial-input function of unchanged radioligand, the stability of [^{18}F]**9** for 2.5 h in whole monkey blood and plasma in vitro was first confirmed by the radio-HPLC method to be used for radiometabolite analysis. This method used a reverse phase column (Novapak C18, 4 [m, 100 × 8 mm; Waters Corp.) within a radial compression module (RCM-100) that was eluted at 2.0 mL/min with MeOH: H_2O: Et_3N (85: 15: 0.1 by vol.). Upon radioligand injection in each of the PET scans in two of the monkeys, arterial blood was sampled into heparin-treated syringes at every 15 s for two minutes followed by further sampling at 3, 5, 10, 30, 60, 75, 90, 120, 150, and 180 min from injection. Plasma [^{18}F]**9** was then quantified in each sample with radio-HPLC, as previously described.[41]

The time course of the plasma concentration of [^{18}F]**9** separated from radiometabolites was used as the input function for compartmental analysis. The total concentration of radioactivity in whole blood was used for vascular correction of the PET data, assuming that blood constitutes 5% of brain volume. The free fraction (f_P) of [^{18}F]**9** in plasma was measured by ultrafiltration, as described previously.[42] Measurements on each plasma sample were made in triplicate.

All monkey images were spatially normalized to a standardized template[43] using a mutual information algorithm (FSL Library, Oxford, UK). Time-activity curves were generated by applying a set of 34 pre-defined region-of-interests on the template. The concentration of radioactivity in each region was expressed as SUV. Time-activity curves were fitted to one and two tissue compartmental models. The two-tissue compartment model was applied to calculate the total distribution volume (V_T) under the three different conditions (baseline, ciproxifan pretreatment and **9** pretreatment). Time-activity curve generation and non-linear parameter fitting was carried out with PMOD 3.0.

Supplementary Material

Refer to Web version on PubMed Central for supplementary material.

Acknowledgments

This study was supported by the Intramural Research Program of the National Institutes of Health (NIMH). We thank the NIH Clinical PET Department (Chief Dr. P. Herscovitch) for fluorine-18 production, and PMOD Technologies for providing the image analysis software. Receptor binding assays were performed by the National Institute of Mental Health's Psychoactive Drug Screening Program, Contract # HHSN-271-2008-00025-C (NIMH PDSP). The NIMH PDSP is directed by Dr. Bryan L. Roth MD, PhD at the University of North Carolina at Chapel Hill and Project Officer Jamie Driscoll at NIMH, Bethesda MD, USA. We also thank Ms. Cheryl L. Morse (NIMH) for assistance in radiochemistry.

Abbreviations

5-HT	serotonin
DAT	dopamine transporter
DMF	*N*,*N*-dimethylformamide
DMSO	dimethyl sulfoxide
f_P	plasma free fraction
GTP	guanosine triphosphate
H_3	histamine subtype-3
HPLC	high performance liquid chromatography

HRMS	high resolution mass spectrometry
NCA	no-carrier-added
NET	noradrenalin transporter
PET	positron emission tomography
RCY	decay-corrected radiochemical yield
SERT	serotonin transporter
SUV	standardized uptake value

References

1. Schwartz JC, Arrang JM, Garbarg M, Pollard H. A third histamine receptor subtype: characterisation, localisation and functions of the H_3 receptor. Agents and Actions. 1990; 30:13–23. [PubMed: 1695431]
2. Cumming P, Shaw C, Vincent SR. High affinity histamine binding site is the H_3 receptor: characterization and autoradiographic localization in rat brain. Synapse. 1991; 8:144–151. [PubMed: 1652795]
3. Pillot C, Heron A, Cochois V, Tardivel-Lacombe J, Ligneau X, Schwartz JC, Arrang JM. A detailed mapping of the histamine H_3 receptor and its gene transcripts in rat brain. Neuroscience. 2002; 114:173–193. [PubMed: 12207964]
4. Leurs R, Bakker RA, Timmerman H, de Esch IJP. The histamine H_3 receptor: from gene cloning to H_3 receptor drugs. Nature Rev Drug Discovery. 2005; 4:107–120.
5. Berlin M, Boyce CW, de Lera Ruiz M. Histamine H_3 receptor as a drug target. J Med Chem. 2011; 54:26–53. [PubMed: 21062081]
6. Yanai K, Tashiro M. The physiological and pathophysiological roles of neuronal histamine: an insight from human positron emission tomography studies. Pharmacol Therapeutics. 2007; 113:1–15.
7. Ponchant M, Demphel S, Fuseau C, Coulomb C, Bottlaender M, Schwartz JC, Stark H, Schunack W, Athmani S, Ganellin R, Crouzel C. Radiosynthesis and biodistribution of two potential antagonists of cerebral histamine H_3 receptors for PET studies: [^{18}F]FUB 272 and [^{11}C]UCL 1829. J Label Compd Radiopharm. 1997; 40:605–607.
8. Windhorst AD, Timmerman H, Menge WMPB, Leurs R, Herscheid JDM. Synthesis, in vitro pharmacology and radiosynthesis of *N*-(*cis*-4-fluoromethylcyclohexyl)-4-(1(H)-imidazol-4-yl)piperidine-1-thiocarbonamide (VUF 5000), a potential PET ligand for the histamine H_3 receptor. J Label Compd Radiopharm. 1999; 42:293–307.
9. Windhorst AD, Timmerman H, Klok RP, Menge WMPB, Leurs R, Herscheid JDM. Evaluation of [^{18}F]VUF 5000 as a potential PET ligand for brain imaging of the histamine H_3 receptor. Bioorg Med Chem. 1999; 7:1761–1767. [PubMed: 10530922]
10. Iwata R, Horvath G, Pascali C, Bogni A, Yanai K, Kovacs Z, Ido T. Synthesis of 3-[1H-imidazol-4-yl]propyl 4-[^{18}F]fluorobenzyl ether ([^{18}F]fluoroproxyfan): a potential radioligand for imaging histamine H_3 receptors. J Label Compd Radiopharm. 2000; 43:873–882.
11. Funaki Y, Sato K, Kato M, Ishikawa Y, Iwata R, Yanai K. Evaluation of the binding characteristics of [^{18}F]fluoroproxyfan in the rat brain for in vivo visualization of histamine H_3 receptor. Nucl Med Biol. 2007; 34:981–987. [PubMed: 17998102]
12. Airaksinen AJ, Jablonowski JA, van der Mey M, Barbier AJ, Klok RP, Verbeek J, Schuit R, Herscheid JDM, Leysen JE, Carruthers NI, Lammertsma AA, Windhorst AD. Radiosynthesis and biodistribution of a histamine H_3 receptor antagonist 4([3-(4-piperidin-1-nyl-but-1-ynyl)-[^{11}C]benzyl]-morpholine: evaluation of a potential PET radioligand. Nucl Med Biol. 2006; 33:801–810. [PubMed: 16934699]

13. Plisson C, Gunn RN, Cunningham VJ, Bender D, Salinas CA, Medhurst AD, Roberts JC, Laruelle M, Gee AD. ^{11}C-GSK189254: a selective radioligand for in vivo central nervous system imaging of H_3 receptors by PET. J Nucl Med. 2009; 50:2064–2072. [PubMed: 19910432]
14. Ashworth S, Rabiner EA, Gunn RN, Plisson C, Wilson AA, Comley RA, Lai RYK, Gee AD, Laruelle M, Cunningham VJ. Evaluation of ^{11}C-GSK189254 as a novel radioligand for the H_3 receptor in humans using PET. J Nucl Med. 2010; 51:1021–1029. [PubMed: 20554726]
15. Hamill TG, Sato N, Jitsuoka M, Tokita S, Sanabria S, Eng W, Ryan C, Krause S, Takenaga N, Patel S, Zeng Z, Williams D Jr, Sur C, Hargreaves R, Burns HD. Inverse agonist histamine H_3 receptor PET tracers labelled with carbon-11 or fluorine-18. Synapse. 2009; 63:1122–1132. [PubMed: 19670309]
16. Cowart M, Faghih R, Curtis MP, Gfesser GA, Bennani YL, Black LA, Pan L, Marsh KC, Sullivan JP, Esbenshade TA, Fox GB, Hancock AA. 4-(2[2-(2(*R*)-methylpyrrolidin-1-yl)ethyl]benzofuran-5-yl)benzonitrile related, 2-aminoethylbenzofuran H_3 receptor antagonists potently enhance cognition attention. J Med Chem. 2005; 48:38–55. [PubMed: 15634000]
17. Pike VW. Positron-emitting radioligands for studies in vivo — probes for human psychopharmacology. J Psychopharmacology. 1993; 7:139–158.
18. Laruelle M, Slifstein M, Huang Y. Relationships between radiotracer properties and image quality in molecular imaging of the brain with positron emission tomography. Mol Imaging Biol. 2003; 5:363–375. [PubMed: 14667491]
19. Patel S, Gibson R. In vivo site-directed radiotracers: a mini-review. Nucl Med Biol. 2008; 35:805–815. [PubMed: 19026942]
20. Pike VW. PET Radiotracers: crossing the blood-brain barrier and surviving metabolism. Trends Pharmacol Sci. 2009; 30:431–440. [PubMed: 19616318]
21. Cai L, Lu S, Pike VW. Chemistry with [^{18}F]fluoride ion. Eur J Org Chem. 2008; 17:2853–2873.
22. Attina M, Cacace F, Wolf AP. Labeled aryl fluorides from the nucleophilic displacement of activated nitro groups by ^{18}F-F$^-$. J Label Compd Radiopharm. 1983; 20:501–514.
23. Feutrill GI, Mirrington RN. Demethylation of aryl methyl ethers with thioethoxide ion in dimethyl formamide. Tetrahedron Lett. 1970:1327–1328.
24. Kubo K, Ohyama S, Shimizu T, Takami A, Murooka H, Nishitoba T, Kato S, Yagi M, Kobayashi Y, Iinuma N, Isoe T, Nakamura K, Iijima H, Osawa T, Izawa T. Synthesis and structure-activity relationship for new series of 4-phenoxyquinoline derivatives as specific inhibitors of platelet-derived growth factor receptor tyrosine kinase. Bioorg Med Chem. 2003; 11:5117–5133. [PubMed: 14604675]
25. Surrey AR. Pyrocyanine in *Org*. Synthesis Collected Volumes. 1955; 3:753.Org Synthesis. 1946; 26:86–90.
26. Kawasaki I, Matsuda K, Kaneko T. Preparation of 1,7-bis(*p*-hydroxyphenyl)heptane. Bull Chem Soc Jpn. 1971; 44:1986–1987.
27. Bjurling, P.; Reineck, R.; Westerberg, G.; Gee, AD.; Sutcliffe, J.; Långström, B. Proc. VIth Workshop on Targetry and Target Chemistry; Vancouver, Canada: TRIUMF; 1995. p. 282-284.
28. Lazarova N, Siméon FG, Musachio JL, Lu S, Pike VW. Integration of a microwave reactor with Synthia to provide a fully automated radiofluorination module. J Label Compd Radiopharm. 2007; 50:463–465.
29. Waterhouse RN. Determination of lipophilicity and its use as a predictor of blood-brain barrier penetration of molecular imaging agents. Mol Imaging Biol. 2003; 5:376–389. [PubMed: 14667492]
30. Zoghbi SS, Anderson KB, Jenko KJ, Luckenbaugh DA, Innis RB, Pike VW. On quantitative relationships between PET radiotracer lipophilicity and plasma free fraction in monkey and human. J Pharm Sci. 2012; 101:1028–1039. [PubMed: 22170327]
31. Cumming P, Laliberté C, Gjedde A. Distribution of histamine H_3 binding in forebrain of mouse and guinea pig. Brain Res. 1994; 664:276–279. [PubMed: 7895042]
32. Jansen FP, Mochizuki T, Maeyama K, Leurs R, Timmerman H. Characterization of histamine H_3 receptors in mouse brain using the H_3 antagonist [^{125}]iodophenpropit. Naunyn- Schmiedeberg's Arch Pharmacol. 2000; 362:60–67.

33. Ligneau X, Lin JS, Vanni-Mercier G, Jouvet M, Muir JL, Ganellin CR, Stark H, Elz S, Schunack W, Schwartz JC. Neurochemcial and behavioral effects of ciproxifan, a potent histamine H_3-receptor antagonist. J Pharmacol Exp Therapeutics. 1998; 287:658–666.
34. Martinez-Mir MI, Pollard H, Moreau J, Arrang JM, Ruat M, Traiffort E, Schwartz JC, Palacios JM. Three histamine receptors (H1, H2 and H3) visualized in the brain of human and non-human primates. Brain Res. 1990; 526:322–327. [PubMed: 1979518]
35. Takano A, Halldin C, Varrone A, Karlsson P, Sjöholm N, Stubbs JB, Schou M, Airaksinen AJ, Tauscher J, Gulyas B. Biodistribution and radiation dosimetry of the norepinephrine transporter radioligand (*S, S*)-[^{18}F]FMeNER-D_2: a human whole-body PET study. Eur J Nucl Med Mol Imaging. 2008; 35:630–636. [PubMed: 18000665]
36. Terry GE, Hirvonen J, Liow JS, Zoghbi SS, Gladding R, Tauscher JT, Schaus JM, Phebus L, Felder CC, Morse CL, Donohue SR, Pike VW, Halldin C, Innis RB. Imaging and quantitation of cannabinoid CB_1 receptors in human and monkey brains using ^{18}. F-labeled inverse agonist radioligands. J Nucl Med. 2010; 51:112–120. [PubMed: 20008988]
37. Clark, JD.; Baldwin, RL.; Bayne, KA.; Brown, MJ.; Gebhart, GF.; Gonder, JC.; Gwathmey, JK.; Keeling, ME.; Kohn, DF.; Robb, JW.; Smith, OA.; Steggerda, J-AD.; VandeBer, JL. Guide for the Care and Use of Laboratory Animals. Washington DC: National Academy Press; 1996.
38. Guillaume M, Luxen A, Nebeling R, Argentini M, Clark JC, Pike VW. Recommendations for fluorine-18 production. Appl Radiat Isot. 1991; 42:749–762.
39. Zoghbi SS, Baldwin RM, Seibyl JP, Charney DS, Innis RB. A radiotracer technique for determining apparent p*K*a of receptor binding ligands. J Label Compd Radiopharm. 1997; 40(S1): 136–138.
40. Briard E, Zoghbi SS, Imaizumi M, Gourley JP, Shetty HU, Hong J, Cropley V, Fujita M, Innis RB, Pike VW. Synthesis and evaluation in monkey of two sensitive ^{11}C-labeled aryloxyanilide ligands for imaging brain peripheral benzodiazepine receptors in vivo. J Med Chem. 2008; 51:17–30. [PubMed: 18067245]
41. Zoghbi SS, Shetty HU, Ichise M, Fujita M, Imaizumi M, Liow JS, Shah J, Musachio JL, Pike VW, Innis RB. PET imaging of the dopamine transporter with [^{18}F]FECNT: a polar radiometabolite confounds brain radioligand measurements. J Nucl Med. 2006; 47:520–527. [PubMed: 16513622]
42. Gandelman MS, Baldwin RM, Zoghbi SS, Zea-Ponce Y, Innis RB. Evaluation of ultrafiltration for the free-fraction determination of single photon emission computed tomography (SPECT) radiotracers: *β*-CIT, IBF, and iomazenil. J Pharm Sci. 1994; 83:1014–1019. [PubMed: 7965658]
43. Yasuno F, Brown AK, Zoghbi SS, Krushinski JH, Chernet E, Tauscher J, Schaus JM, Phebus LA, Chesterfield AK, Felder CC, Gladding RL, Hong J, Halldin C, Pike VW, Innis RB. The PET radioligand [^{11}C]MePPEP binds reversibly and with high specific signal to cannabinoid CB_1 receptors in nonhuman primate brain. Neuropsychopharmacology. 2008; 33:259–269. [PubMed: 17392732]

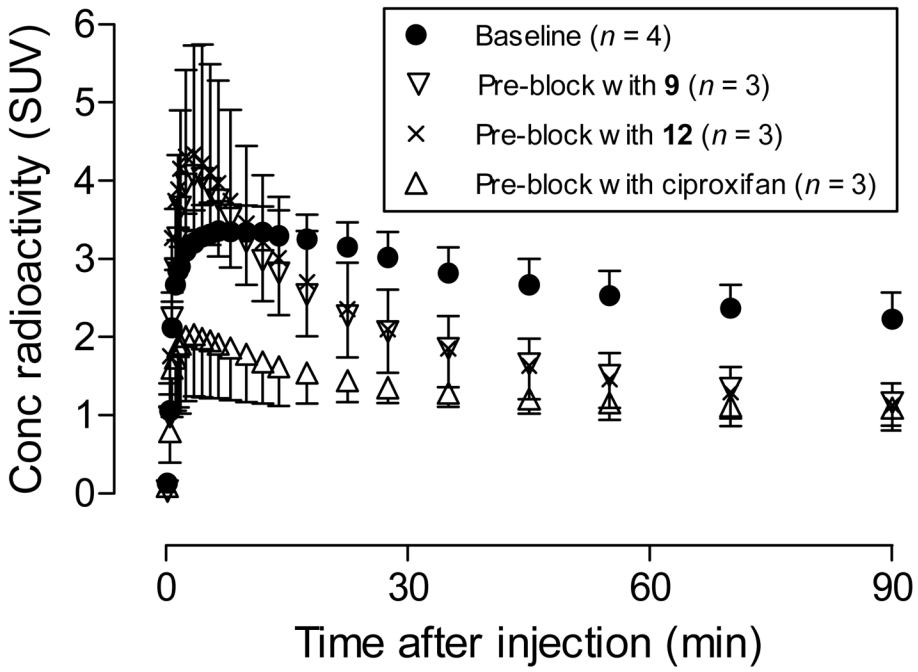

Figure 1.
Whole brain time-activity curves after [^{18}F]**9** was injected in mice under baseline and pre-treatment conditions. Data points are means with one-sided error bars showing SD.

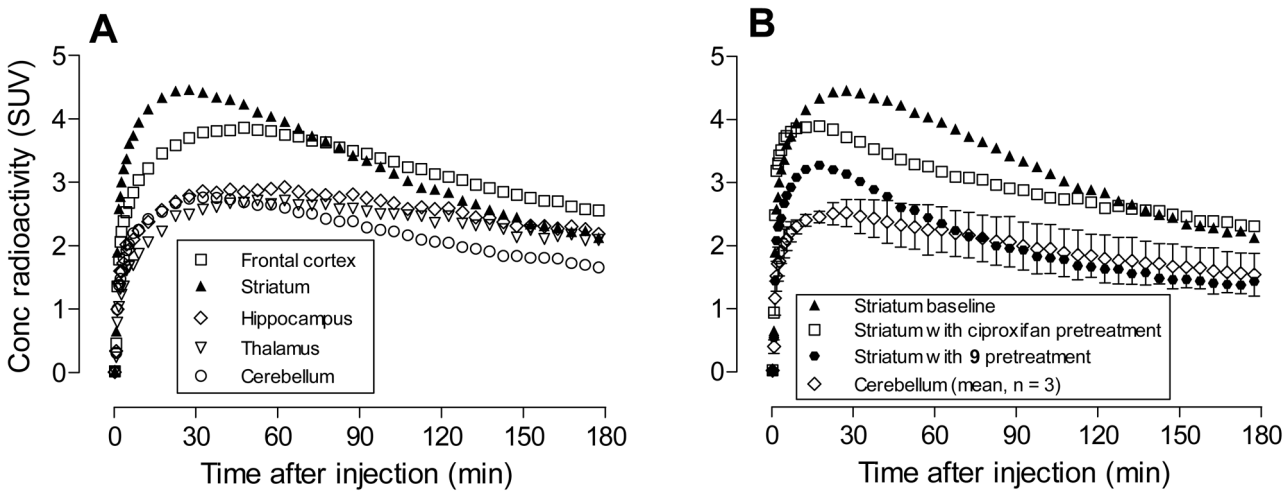

Figure 2.

Brain region time-activity curves after [^{18}F]**9** was injected intravenously into monkey at baseline (Panel A). Panel B shows the effect of pretreatment with either ciproxifan (2.0 mg/kg, i.v.) or **9** (1 mg/kg, i.v.) on the time-activity curve for striatum. The mean curve for cerebellum from the three experiments is shown for comparison. Error bars represent mean ± SD.

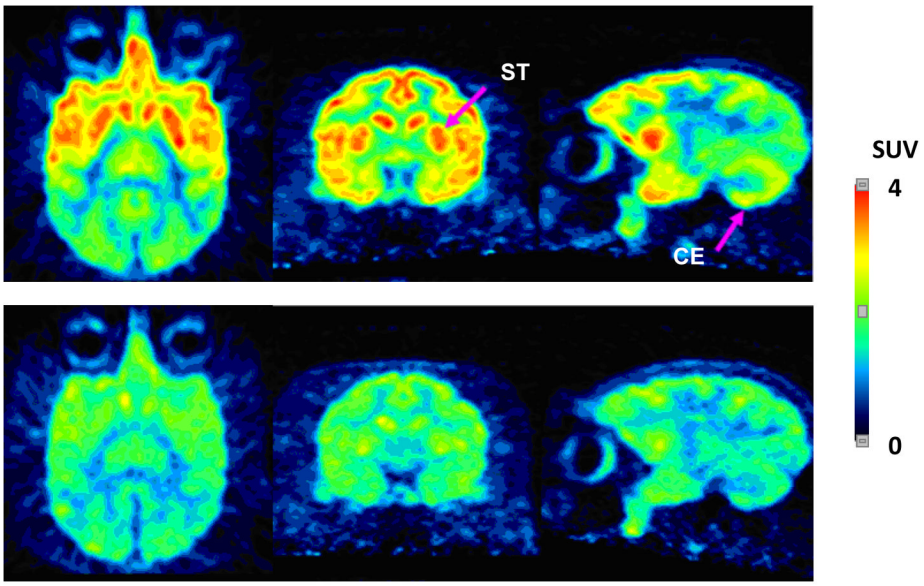

Figure 3.

Axial, coronal and sagittal PET images of brain through the striatum, after intravenous injection of a monkey with [^{18}F]**9** at baseline (top panel) and after pre-treatment with **9** (1.0 mg/kg, i.v.) (bottom panel). Images were acquired for 180 min immediately after each radioligand injection.

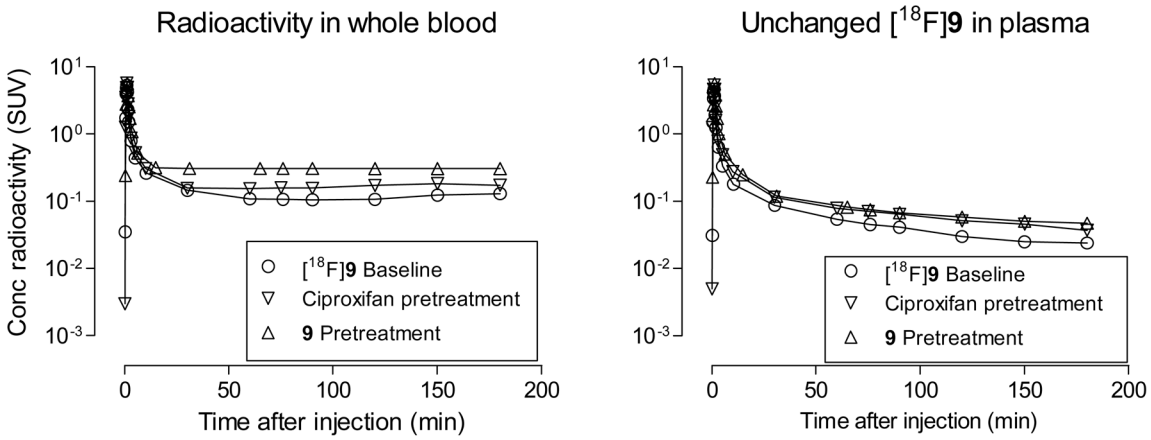

Figure 4.

Time course of plasma concentration (SUV) of total radioactivity and unchanged [^{18}F]**9** after intravenous injection of [^{18}F]**9** into a rhesus monkey, under baseline, ciproxifan-pretreatment and **9**-pretreatment conditions..

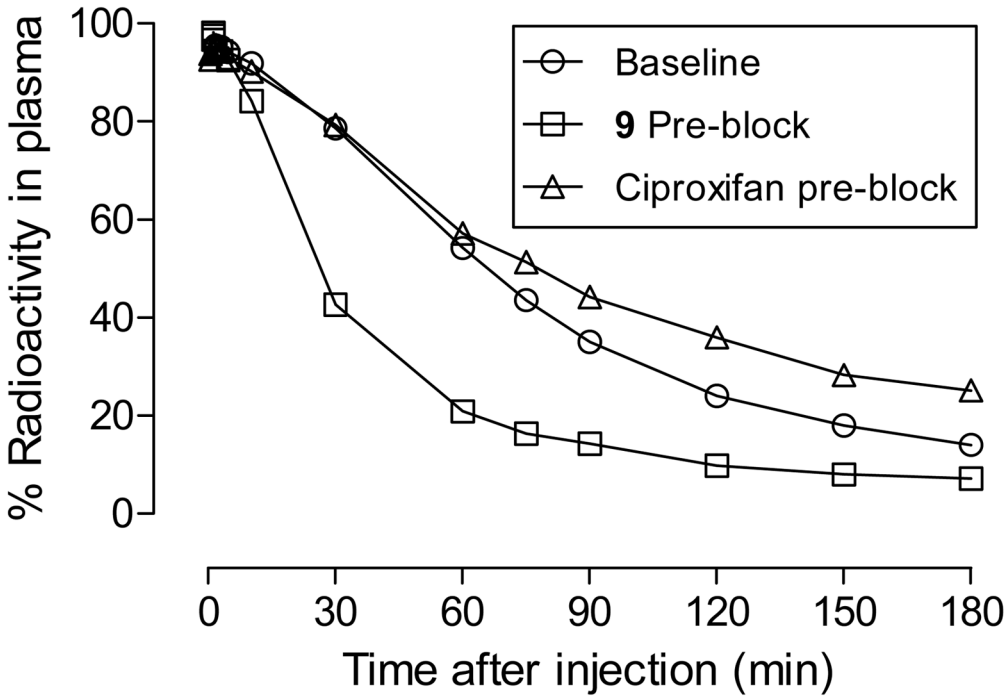

Figure 5.
Percentage of radioactivity in plasma represented by unchanged radioligand after injection of a monkey with [^{18}F]**9** at baseline, after treatment with **9**, and after treatment with ciproxifan. The remainder of radioactivity was composed of radiometabolites [^{18}F]**A-C**.

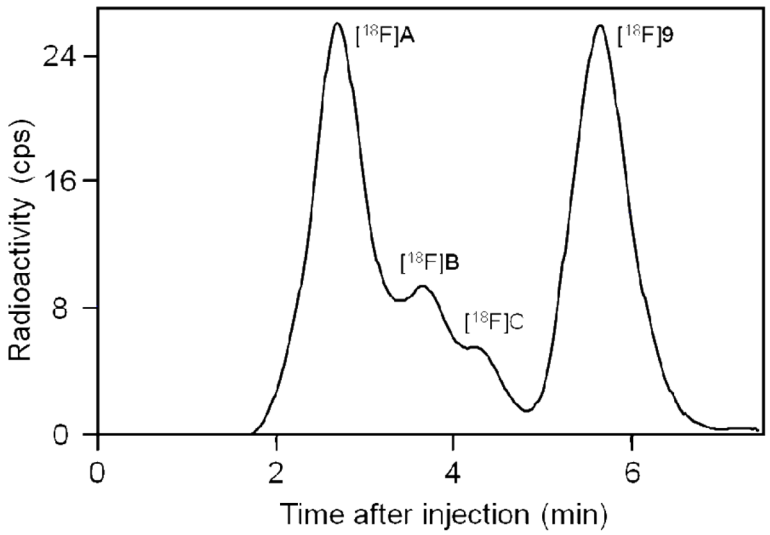

Figure 6.
Reverse phase HPLC radiochromatogram of plasma sampled from monkey at 75 min after intravenous injection of [^{18}F]**9** (3.87 mCi). See text for details of analysis.

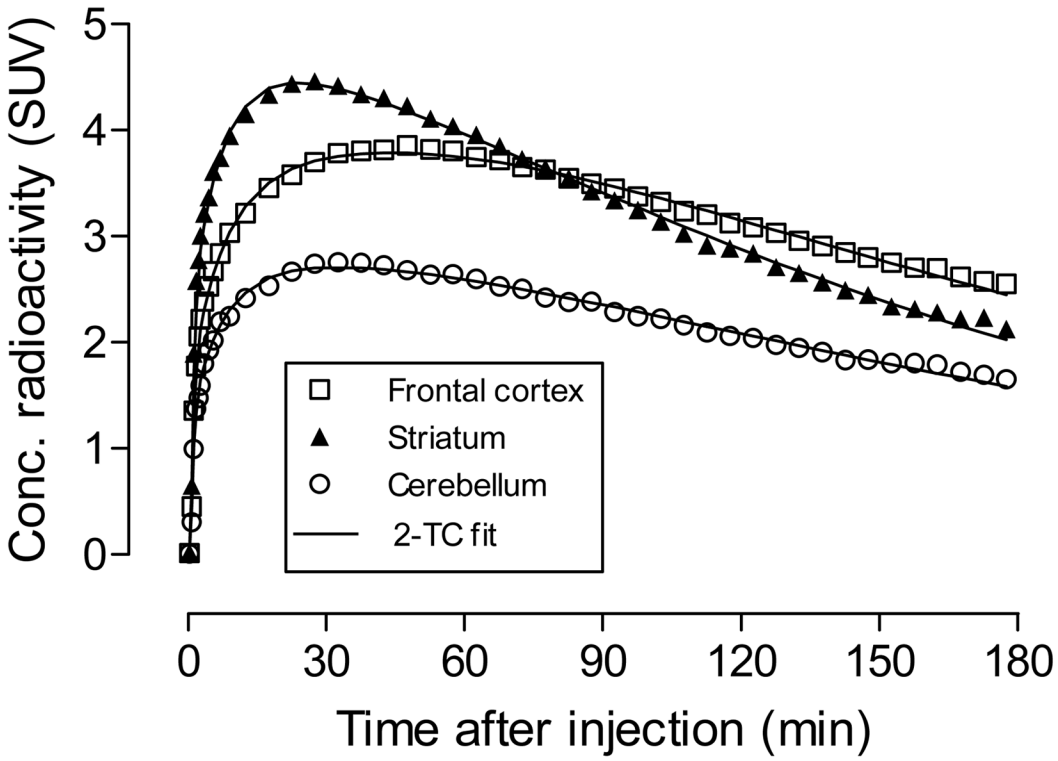

Figure 7.
Fitting to 2-tissue compartmental models of time-activity curves acquired in three brain regions after i.v. injection of monkey with [^{18}F]**9**.

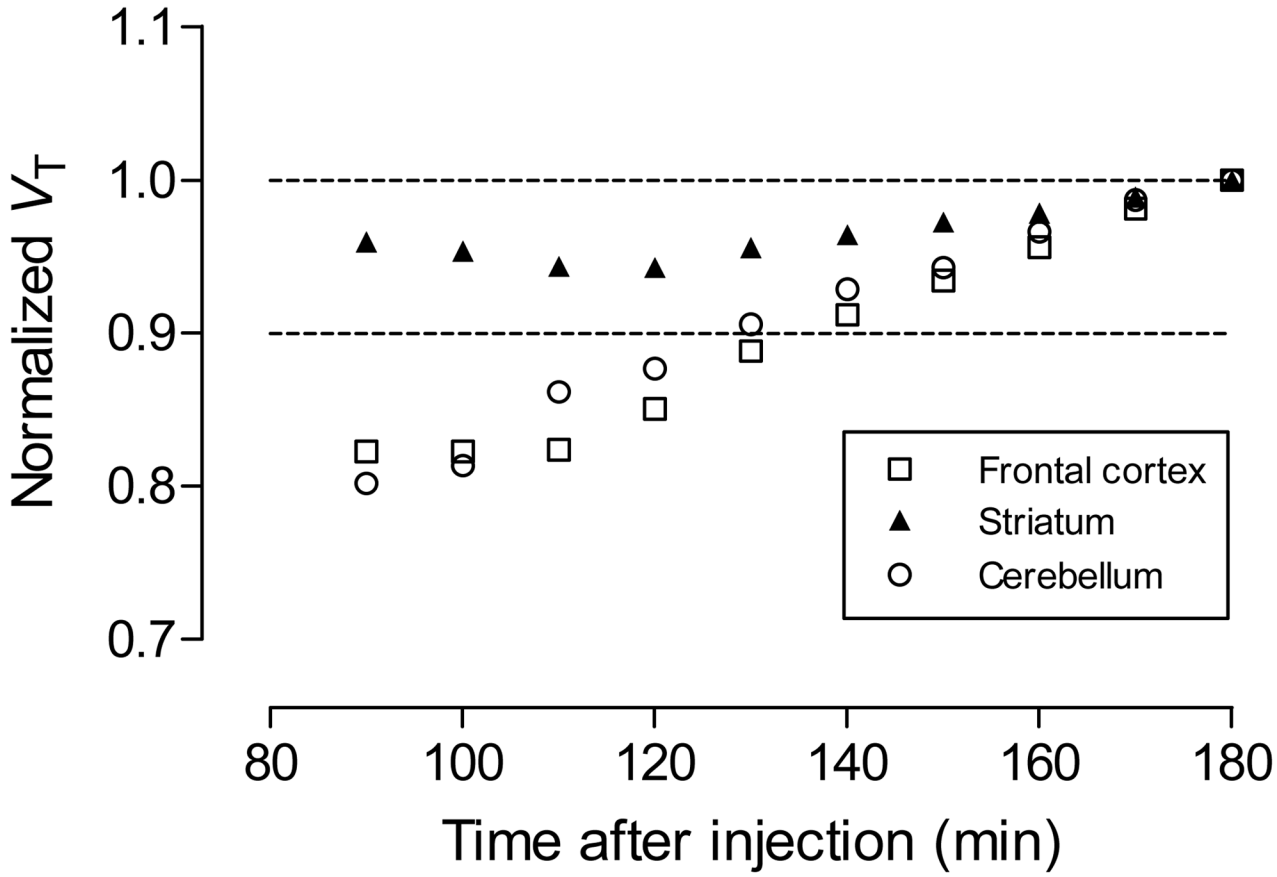

Figure 8.
Time stability of normalized total volume of distribution (V_T) determined in three regions in one monkey with [^{18}F]**9**. Each V_T value was estimated from only the PET data collected up to that time-point.

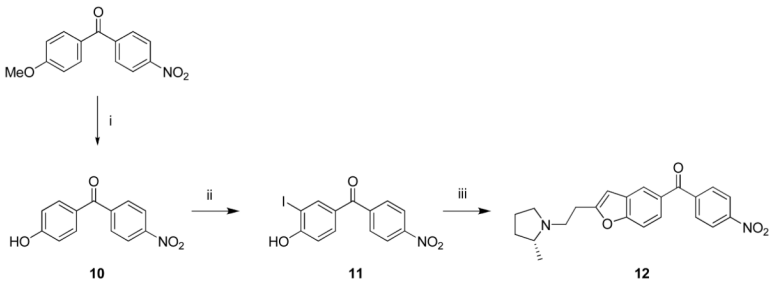

Scheme 1. Synthesis of nitro precursor 12

Reagents, conditions and yields: (i) HBr, AcOH, reflux, 9 h; 87%; (ii) I_2, KI, NH_4OH, rt, 48 h; 26%; (iii) a) 1-(3-butynyl)-2-(*R*)-methylpyrrolidine, $Pd(OAc)_2$, (*p*-tol)$_3$P, CuI, rt, 10 min; b) *i*-Pr_2NH, MeCN, 60 °C,16 h; 28%.

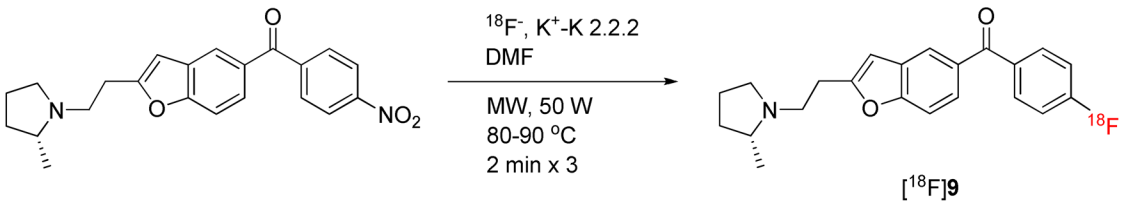

[18F]**9**

Scheme 2.
Radiosynthesis of [18F]**9**.

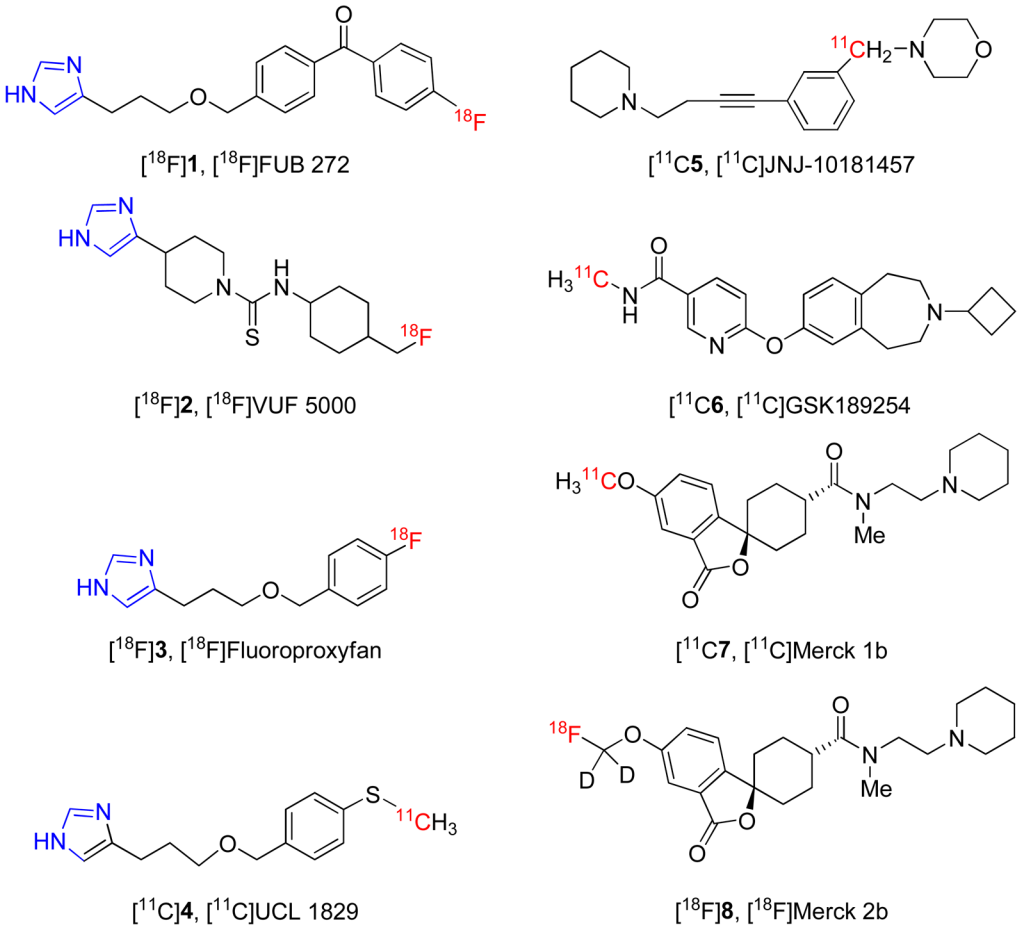

Chart 1.

Previously reported PET radioligands for H_3 receptors; imidazole-based radioligands are shown on the left and non-imidazole-based radioligands on the right

Table 1

K_i values of compounds **9** and **12** determined from *in vitro* competitive binding assays.

Receptor or binding site	K_i (nM)	
	9	**12**
H_1	5,440	7,055
H_2	1,708	923
H_3	1.9 ± 0.23	0.4 ± 0.04
H_4	>10,000	>10,000
5-HT_{1A}	432	>10,000
5-HT_{1B}	>10,000	>10,000
5-HT_{1D}	6,380	5,237
5-HT_{2A}	2,718	1,355
5-HT_{2B}	3,152	>10,000
DAT	>10,000	137
M_1	3,266	931
M_2	462	681
M_3	204	512
M_4	351	415
M_5	437	336
All others[a]	>10,000	>10,000

[a] 5-HT1E,2C,3,5A,6 and 7, α1A,1B,1D,2A,2B and 2C, β1–3, D1–5, σ1,2, SERT and NET

Table 2

Estimation of V_T from 2TC model in two monkeys injected with [^{18}F]**9** at baseline, after treatment with ciproxifan and after treatment with **9**.

Region	Monkey# 1 V_t			Monkey# 2 V_t			Mean V_t decrease (%)	
	Baseline	Ciproxifan pretreatment	9 pretreatment	Baseline	Ciproxifan pretreatment	9 pretreatment	Ciproxifan	9 pretreatment
Frontal cortex	64.1	43.5	29.5	42.1	26.7	16.4	-34	-58
Striatum	54.7	42.7	29.1	45.3	31.6	19.7	-26	-52
Hippocampus	60.4	45.3	31.2	50.8	30.4	20.8	-33	-54
Thalamus	53.7	40.8	29.9	49.9	29.4	19.4	-33	-53
Cerebellum	42.0	33.5	24.8	28.5	19.6	12.0	-26	-49